An Inline V-Band WR-15 Transition Using Antipodal Dipole Antenna as RF Energy Launcher @ 60 GHz for Satellite Applications

Atul Varshney [1][ID], Vipul Sharma [1], Issa Elfergani [2,3,*][ID], Chemseddine Zebiri [4][ID], Zoran Vujicic [3] and Jonathan Rodriguez [3,5]

1   ECE Department, FET Gurukula Kangri (Deemed to Be) University, Haridwar 249404, India
2   The Instituto de Telecomunicações, Campus Universitário de Santiago, 3810-193 Aveiro, Portugal
3   School of Engineering and Informatics, University of Bradford, Bradford BD7 1DP, UK
4   Laboratoire d'Electronique de Puissance et Commande Industrielle (LEPCI), Department of Electronics, University of Ferhat Abbas, Sétif -1-, Sétif 19000, Algeria
5   Faculty of Computing, Engineering and Science, University of South Wales, Pontypridd CF37 1DL, UK
*   Correspondence: i.t.e.elfergani@av.it.pt or i.elfergani@bradford.ac.uk

Abstract: This article demonstrates the design and development of WR-15 transition using an antipodal microstrip dipole antenna at a frequency of 60 GHz for space applications. An inline microstrip line to rectangular waveguide (MS-to-RWG) transition is proposed for the V-band (50–75 GHz) functioning. The RF energy is coupled and launched through an antipodal dipole microstrip antenna. Impedance matching and mode matching between the MS line and dipole are achieved by a quarter wave impedance transformer. This results in the better performance of transitions in terms of insertion loss (IL > −0.50 dB) and return loss (RL < −10 dB) for a 40.76% relative bandwidth from 55.57 GHz to 65.76 GHz. The lowest values of IL and RL at 60 GHz are −0.09 dB and −32.05 dB, respectively. A 50 μm thick double-sided etched InP substrate material is used for microstrip antipodal dipole antenna design. A back-to-back designed transition has IL > −0.70 dB and RL < −10 dB from 54.29 GHz to 64.07 GHz. The inline transition design is simple in structure, easy to fabricate, robust, compact, and economic; occupies less space because the transition size is exactly equal to the WR-15 length; and is prepared using an InP substrate with high permittivity of 12.4 and thickness of 50 μm. Thus, the devices have the lowest insertion loss value and lowest return loss (RL) value, of <−31 dB, as compared to earlier designs in the literature. Therefore, the proposed design has the lowest radiation loss (because of thickness) and highest transmission (about 97% power). Easy impedance matching using only a single-step quarter-wave transformer between the antipodal dipole antenna and 50 Ω microstrip line (avoiding the multi-sections' demand and microstrip line's tedious complexity) is needed. Since, when the InP dielectric substrate is inserted in WR-15, the waveguide becomes a dielectric-filled waveguide (DFWG), and its characteristics impedance reduces to 143 Ω from 505 Ω at an operating frequency of 60 GHz. In the proposed transition, no ridge waveguide or waveguide back-short is utilized in WR-15. The microstrip line did not contain any via, fence, window, screw, galvanic structure, post, etc. Hence, the transition is suitable for high-data-rate 5G communications, satellite remote sensing, missile navigation, MIC/MMIC circuits' characterization, and mm-wave applications. The electrical equivalent model of the proposed design has been generated and validated using an RF circuit simulator and was found to have excellent matching.

Keywords: electrical equivalent circuit model; interconnects; microstrip line; mm-waves; V-band; WR-15 transition

1. Introduction

The high data rates necessary for MMIC, HMIC, MIC, MIMO, and massive MIMO require new types of inline (0°) [1–10] and vertical (90°) [11–20] interconnects between

dissimilar transmissions lines [21,22]. Previously, most of the MS-to-RWG hybrid transitions have been designed using a ridge waveguide structure [7,8] or using a waveguide back-short [16,18] or multi-layered [3,22] complex microstrip lines in the microwave L-band, S-band, C-band, X-band, Ku-band, K-band, Ka-band, Q-band, and W-band. Very little information in the literature is available regarding V-band and U-band MS-to-RWG transitions for mm-wave applications [18,23,24]. This motivates and attracts the researchers' focus to work in this 50–75 GHz range of MS-to-RWG transitions. Previously designed V-band transitions use the costly Roger/RT Duroid 5880 as the substrate, with a thickness between 5 mils (0.127 mm) and 10 mils (0.254 mm) and a low permittivity value of 2.2 [18,23]. Thus, these transitions are costlier, are bigger in size, and have high radiation losses, poor transmission, and reflection coefficient values. In 1988, Shih, Y. C. et al. invented the first V-band transverse MS-to-RWG transition for mm-wave and MMIC applications. The microstrip is inserted into the waveguide by aperture cut, and the microstrip probe is used as the launching element. The invented transition has IL > −1.0dB and RL < −12 dB over a relative bandwidth of 40% [18]. Aliakbarian et al. have presented an end wall inserted transverse double-slot MS-to-RWG transition. The microstrip uses double-sided etched RT droid 5880 substrates. The fabricated transition has better RL over a wide fractional bandwidth (FBW) of 37.7%, but it has a poor IL of −4.0 dB [23]. Zhou, I. and Robert, J. R. have designed and validated an inline narrow-wall MSL-to-RW transition B2B configuration. The designed transition can work for both the top side and bottom side simultaneously without increased manufacturing complexity. The transition consists of an MS line that feeds an array of three overlapped transversal patches from the narrow wall of the RWG, offering an FBW of 21.2% for the top-side design and 23% for the bottom-side design, with IL from 0.40 dB to 0.70 dB for filling the Local Multipoint Distribution Service (LMDS) and Ka-band operations [25]. Kyu, Y.H. and Pao, C. have designed an inline E-plane probe wideband, low loss V-band MS-to-WR15 transition using a quartz substrate using a five-step ridge waveguide. The ridge waveguide and the microstrip lines are fully integrated into the same housing. The transition has IL < 0.7dB (B2B) over the 50 GHz to 72 GHz band [26]. Mozharovskiy, A. V. et al. have designed and investigated a 60 GHz transverse low-loss wideband probe type MSL-to-RWG transition using the CPS SIW section surrounding the probe. The transition results in IL > −1.1dB (RO4350B) for FBW 11.2% and IL > −0.70 dB (RT Duroid 5880) for FBW 20% [27]. Xu, Z. et al. have demonstrated an E-plane probe-fed T-junction structure using an inline W-band MS-to-RWG back-to-back transition for mm-wave applications. The MS line is fabricated on a quartz substrate, and a two-step transformer is used between the 50 Ω MS feed and MS probe with symmetric wings structure for impedance and field-matching purposes. The transition has 1.0dB IL and RL better than −10dB over the entire W-band [28]. Henderson, J. R. and Walden, M. C. have demonstrated a PCB edge transition to feed an H-plane sectoral horn array for 3D-printed mm-wave beam-forming devices. The transition is designed at 64 GHz having IL > −1.0dB over FBW 21.87% [29,30].

The main objective of this work is to achieve low radiation losses, an excellent impedance match, and a mode match between two dissimilar transmission lines (quasiTEM mode and TE mode). The purpose of doing so is to get a better return loss of <−10 dB and insertion loss >−1 dB for a good range of fractional/relative bandwidth. Another objective of this work is to design an economic, simple, compact, robust, waveguide back-short without via, fence, and ridge waveguide MS-to-RWG interconnects for the front end of an mm-wave transmitter and receiver that could operate sharply at the center frequency of 60 GHz for the V-Band.

This paper describes the design and development of an economic, simple structured, easy-to-fabricate microstrip line and a microstrip line to rectangular waveguide transition for V-band (50 GHz–75 GHz) space applications. This transition consists of a microstrip antipodal dipole antenna as an RF energy launcher. IL and RL performance parameters are achieved at a center frequency of 60 GHz with a single impedance transformer.

2. Materials and Methods

An inline microstrip to rectangular waveguide (MS-to-RWG) transition is designed at an operating frequency of 60 GHz for V-band operations. A compact piece of perfect electric conductor (PEC) rectangular waveguide WR-15 with dimensions 3760 μm × 1880 μm of length 5000 μm is chosen at an operating frequency of 60 GHz. A metal pedestal of dimensions 1880 μm × 1880 μm × 2500 μm is placed inside WR-15 at one end of the waveguide to support a 50 μm thick Indium Phosphide (InP) substrate. The two arms (80 μm × 676 μm) of the dipole antenna are printed on the opposite sides of the substrate. A quarter wave (λ/4) impedance-matching transformer is used between the 50 Ω microstrip line and the dipole arms to match the impedance. No waveguide back-short or ridge waveguide structure with other dielectrics is filled within the RWG. A low-loss high-frequency InP substrate of thickness 50 μm is selected for the microstrip patch antenna. The InP substrate has a permittivity of 12.4 and a loss tangent of 0.0001 at 60 GHz. The width of the substrate is just kept at 80 μm less than the width of the waveguide, and the length of the substrate is the sum of the lengths of the 50 Ω microstrip line (MSL) and the length of the quarter-wave impedance transformer. The microstrip dipole antenna is used for RF energy coupling in a waveguide (WR-15). No ground layer is printed on the substrate bottom; thus, the metal pedestal plays the role of ground for microstrip quasi-TEM mode. The mode matching between the microstrip line and the waveguide transverse electric dominating mode TE_{10} is achieved by symmetrically adjusting the length and width of arms of the antipodal dipole microstrip antenna. The dipole arm dimensions of the antenna are evaluated using a rectangular patch by the general equations [31]. The following design Equations (1)–(16) are used for the proposed transition design using a dipole antenna as a launcher.

Total Length of the dipole antenna

$$L_d = \lambda_d = \frac{0.468\lambda}{\sqrt{\varepsilon_{eff}}} \tag{1}$$

where

$$\varepsilon_{eff} = \frac{\varepsilon_r + 1}{2} + \frac{\varepsilon_r - 1}{2}\left[\left(1 + 12\frac{h}{w}\right)^{-0.5} + 0.04\left(1 - \frac{w}{h}\right)^2\right] \tag{2}$$

Length of each arm of the dipole antenna

$$L_{D1} = L_{D2} = \frac{\lambda_d}{2} \tag{3}$$

Width of each arm of the dipole antenna

$$W_{D1} = W_{D2} = 0.01\lambda \tag{4}$$

Length of the impedance transformer

$$L_t = \frac{\lambda}{4} \tag{5}$$

Substrate width

$$W_{sub} = b - 80 \tag{6}$$

Substrate length

$$L_{sub} = L_{MS} + L_t \tag{7}$$

50 Ω microstrip line (MSL) length and width

$$L_{MS} = L_F = \frac{\lambda}{2} \tag{8}$$

$$W_f = \frac{7.48h}{e^{\left(Z_0 \frac{\sqrt{(\varepsilon_r + 1.41)}}{87}\right)}} - 1.25t \tag{9}$$

Half-wave dipole antenna impedance $Z_{dipole} = 73.4\ \Omega$

Impedance of impedance transformer [32]

$$Z_t = \sqrt{Z_{MS} \cdot Z_{dipole}} \tag{10}$$

Width of the impedance transformer [33]

$$W_t = \frac{7.48h}{e^{\left(Z_{dipole} \frac{\sqrt{(\varepsilon_r + 1.41)}}{87}\right)}} - 1.25t \tag{11}$$

Length of waveguide

$$L_{WG} \geq \lambda \tag{12}$$

Height of metal pedestal

$$H_{gnd} = \frac{a}{2} \tag{13}$$

Length of metal pedestal

$$L_{gnd} = \frac{\lambda}{2} \tag{14}$$

Width of metal pedestal

$$w_{gnd} = b \tag{15}$$

Impedance of air-filled WR-15 (RWG) for TE_{10} mode [34]

$$Z_{WG} = \frac{\eta}{\sqrt{1 - \left(\frac{f_c}{f_0}\right)^2}} \tag{16}$$

The design structure of the inline transition of the MSL-to-RWG transition is shown in Figure 1. The RF energy is launched by the microstrip line. For this purpose, the mm-wave microstrip antenna was designed to operate within the frequency band (V-band, 50 GHz to 75 GHz). The microstrip antenna in this transition is an essential part to launch RF energy into the RWG (WR-15). The designed microstrip antipodal antenna structure, at a frequency of 60 GHz, is shown in Figure 2. The dimensional description of the design has been depicted in Table 1. All dimensions are measured in micrometers (μm).
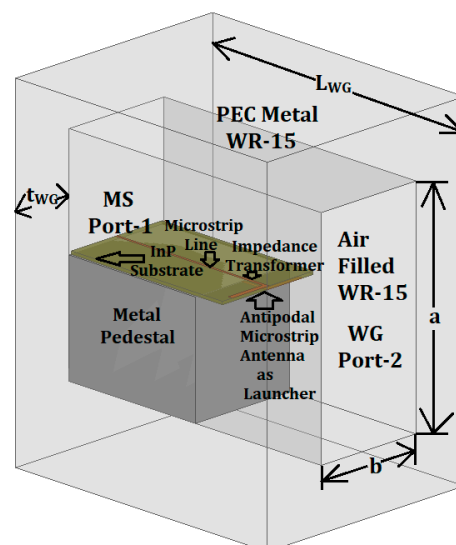
Figure 1. V-band inline transition of the MSL-to-RWG transition.
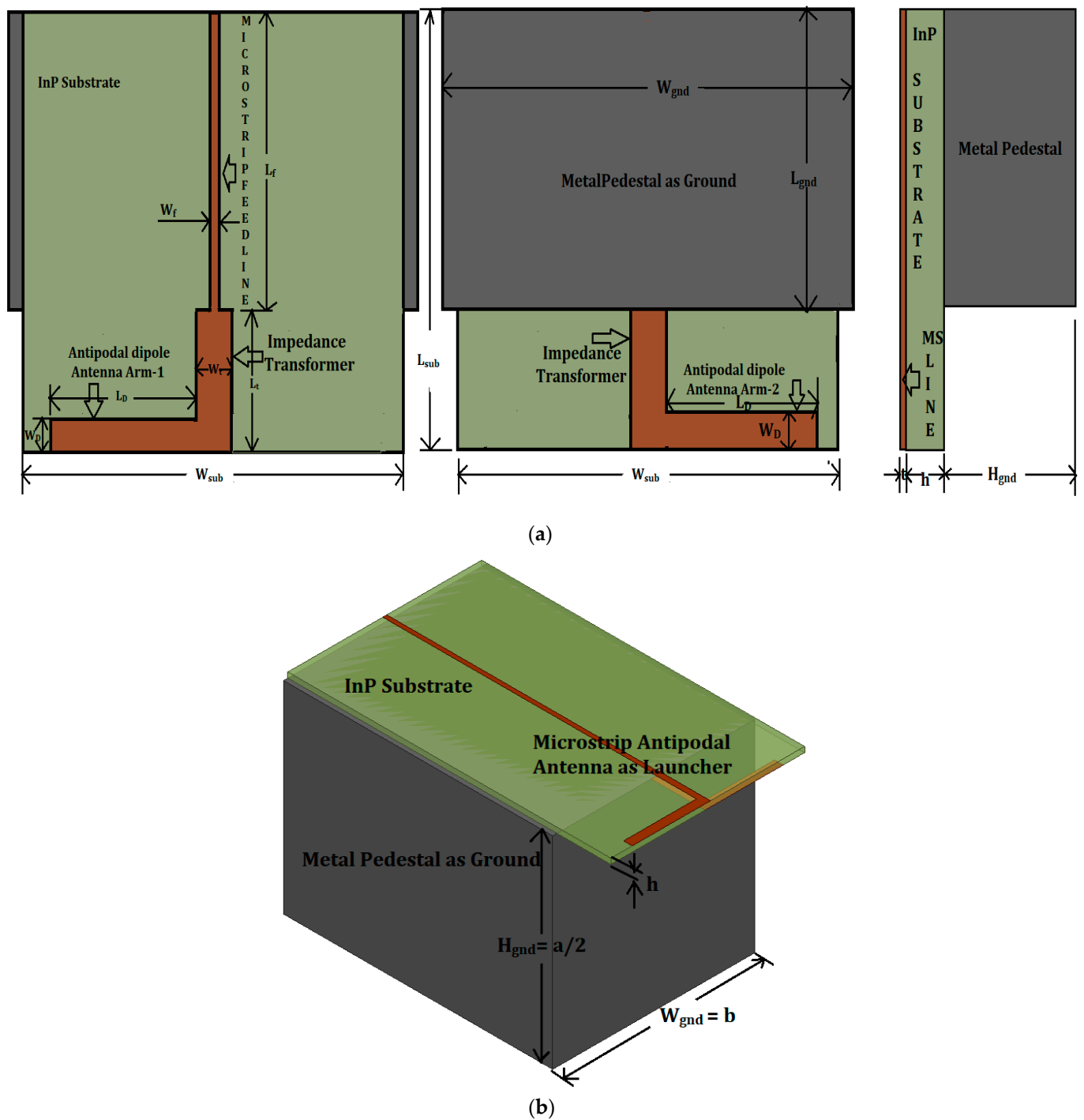
Figure 2. Microstrip antipodal dipole antenna as RF energy launcher for V-band transitions. (**a**) Front view, rear view, and side view; (**b**) microstrip line.

Table 1. Dimensions of the designed MSL-to-RWG waveguide transition.

Parameter Name	Parameter Designation	Dimensions Values (μm)
RWG	WR-15 inner dimensions: Breadth: a Width: b Length: L_{WG} Thickness: t_{WG}	WR-15 inner dimensions: a: 3760 b: 1880 L_{WG}: 5000 t_{WG}: 1015
PEC Metal Pedestal (Ground)	Width: W_{gnd} Height: H_{gnd} Length: L_{gnd}	W_{gnd} : $b = 1880$ H_{gnd} : $\frac{a}{2} = 1880$ L_{gnd} : $\frac{L_{WG}}{2} = 2500$
Substrate	Width: W_{sub} Length: L_{sub} Height: H_{sub}	W_{sub}: b-80 = 1800 L_{sub} : $L_{MS} + L_t = 3000$ H_{sub}: 50
50Ω MSL	Feed width: W_f Feed length: L_f Thickness: t	W_f: 37.79 L_f: 2500 t: 400nm (gold)
Impedance Transformer	TF width: W_t TF length: L_t Thickness: t	W_t: 50 L_t: 500 t: 400 nm (gold)
Microstrip Dipole Antipodal Antenna	Dipole arms: Width: W_D Length: L_D Thickness: t	Probe/dipole: W_D: 80 L_D: 676 t: 400 nm (gold)

2.1. Substrate-Width Variations of V-Band Inline Transitions

Initially, the substrate width was kept equal to the waveguide width, and then the substrate width is varied in a step of 80 μm. It is observed in this process that if the substrate width reduces, then it results in a shift in frequency toward the right, and return loss becomes reduced without affecting the relative bandwidth and vice versa, as illustrated in Figure 3 and displayed in Table 2.
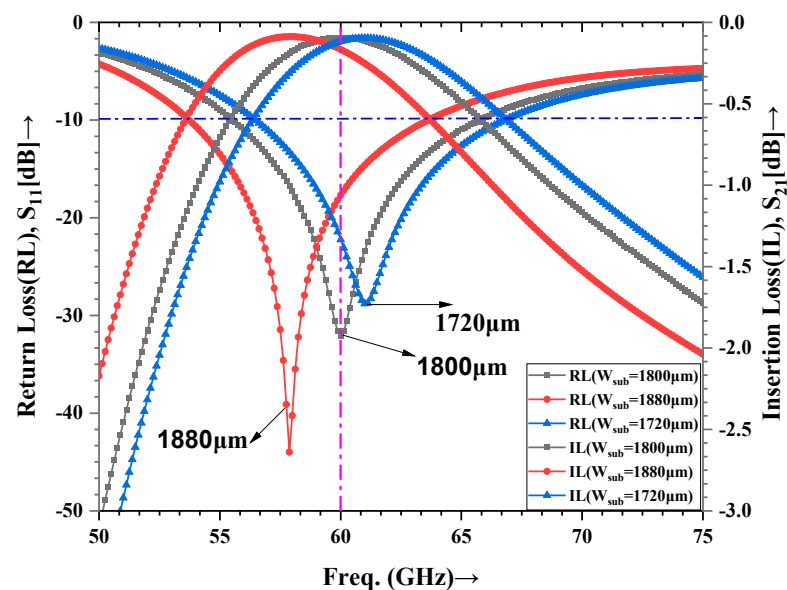
Figure 3. Effect of variations of substrate width on RL and IL plots.

Table 2. Substrate width variations.

Substrate Width, W_{sub} (µm)	Tuning Frequency (GHz)	RL (dB)	IL (dB)	−10dB Bandwidth (GHz)
1720	61.07	−28.75	−0.10	56.48–66.79
1800	60	−32.05	−0.09	55.54–65.72
1880	57.90	−44.19	−0.09	53.73–63.64

2.2. Length Variations of Dipole Antenna Arms

The initial evaluated arms' length of the dipole antenna using Equations (1)–(3) is 431.68 µm; with this value for the dipole's arms, no significant results in terms of RL, IL, and FBW were obtained. The best IL of −0.09 dB and RL of −32.05 dB were obtained at frequency 60 GHz with dipole arms of width 676 µm. Thus, all other dimensions of the MS-to-WG transition were kept constant (with substrate width 1800 µm), and the arms' length of the dipole was varied in a step size of 80 µm. The dipole length is varied in 626 µm, 676 µm, and 726 µm steps. It is observed in this process that if the dipole antenna arms' length reduces, then the resonant frequency shifts toward the right. The lowest return loss of −32.05 dB and insertion loss of −0.09 dB were obtained at the designed frequency of 60 GHz, as illustrated in Figure 4 and displayed in Table 3.
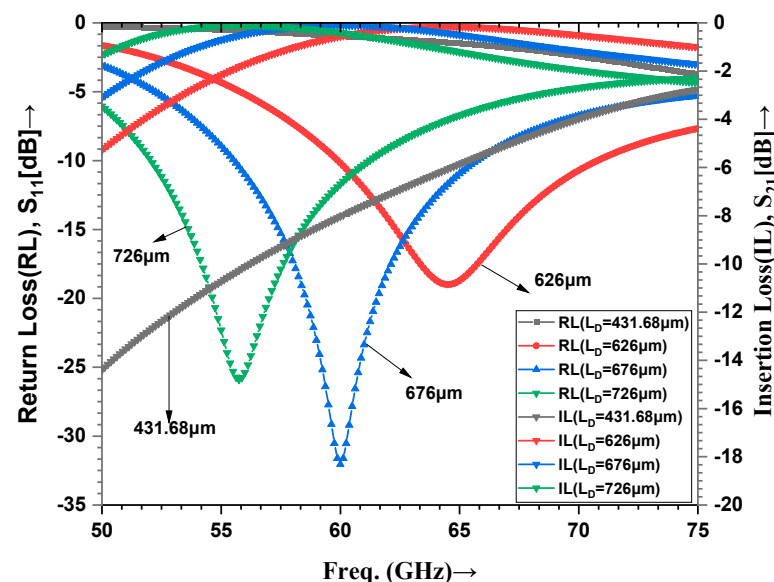
Figure 4. Effect of variations of dipole antenna length on RL and IL plots.

Table 3. Dipole antenna arms' length variations.

Dipole Antenna Arms' Length, L_D (µm)	Tuning Frequency (GHz)	RL (dB)	IL (dB)	−10 dB Bandwidth (GHz)
431.68	– – – – – – – – –	– – – – – – – – –	– – – – – – – – –	– – – – – – – – –
626	64.57	−19.06	−0.15	59.90–70.79
676	60	−32.05	−0.09	55.54–65.72
726	55.75	−25.88	−0.10	52.06–61.22

2.3. Width Variations of Dipole Antenna Arms

The initial evaluated arms' width of the antipodal dipole antenna using Equation (4) is 50 µm. The best IL of −0.09 dB and RL of −32.05 dB were obtained at frequency 60 GHz with dipole arms' width of 80 µm, as illustrated in Figure 5 and displayed in Table 4. Thus, all other dimensions of the MS-to-WG transition were kept constant (with substrate width 1800 µm), and the arms' width of the dipole was varied in a step size of 30 µm. The dipole width is varied in 20 µm, 50 µm, 80 µm, and 110 µm steps. In this process, it is observed

that if the dipole antenna arms' width increased from 20 μm, then it improves the mode matching at frequency 6 GHz between the quasi-TEM mode of microstrip line and TE_{10} mode of rectangular waveguide. Resonant frequency does not very much affect the change in dipole width after 50 μm, but return loss becomes reduced. Change in dipole width does not affect the tuning frequency of the transition.
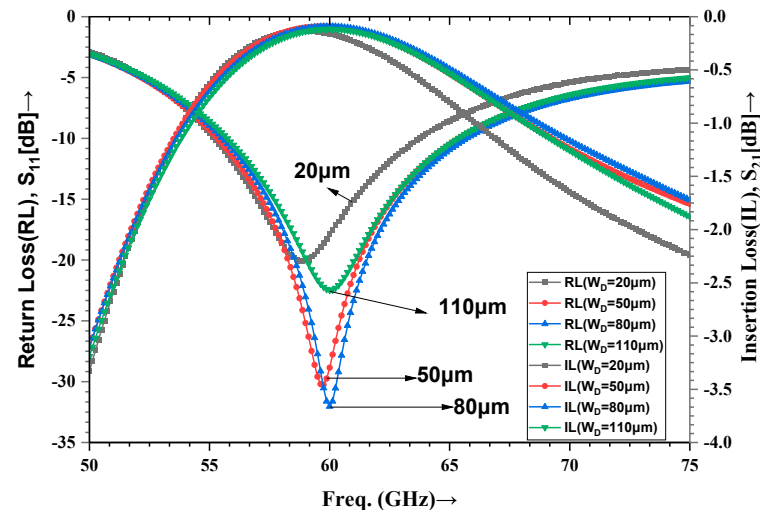
Figure 5. Effect of variations of dipole antenna length on RL and IL plots.

Table 4. Dipole antenna arms' width variations.

Dipole Antenna Arms Width, W_D (μm)	Tuning Frequency (GHz)	RL (dB)	IL (dB)	−10 dB Bandwidth (GHz)
20	58.82	−20.08	−0.13	55.19–63.73
50	64.57	−30.41	−0.09	55.33–65.40
80	60	−32.05	−0.09	55.54–65.72
110	60	−22.47	−0.12	55.74–65.35

3. Results

A back-to-back transition for the MS line to the waveguide for the V-band is shown in Figure 6. The RL and IL plots of conventional and back-to-back (B2B) MS line-to-RWG transitions at the V-band are represented in Figure 7 and compared in Table 5. It is concluded from the comparison of the plot results that the conventional MS-to-WG transition has IL close to −0.1 dB that guarantees maximum transmission at 60 GHz and excellent impedance matching over −10 dB FBW (55.57–65.76 GHz). On the other hand, when this transition is connected B2B, the lowest IL of −0.13 dB, −0.12 dB, and −0.18 dB and RL og −39.77 dB, −67.53 dB, and −35.36 dB have been achieved at frequencies 55.25 GHz, 60.87 GHz, and 69.13 GHz, respectively. Therefore, B2B transition is triple-tuned in the dual band from 50 GHz to 75 GHz. The use of this technique could be generalized for the design and fabrication of microwave and mm-wave band MS-to-RWG Transitions for applications from 1 GHz to 325 GHz.
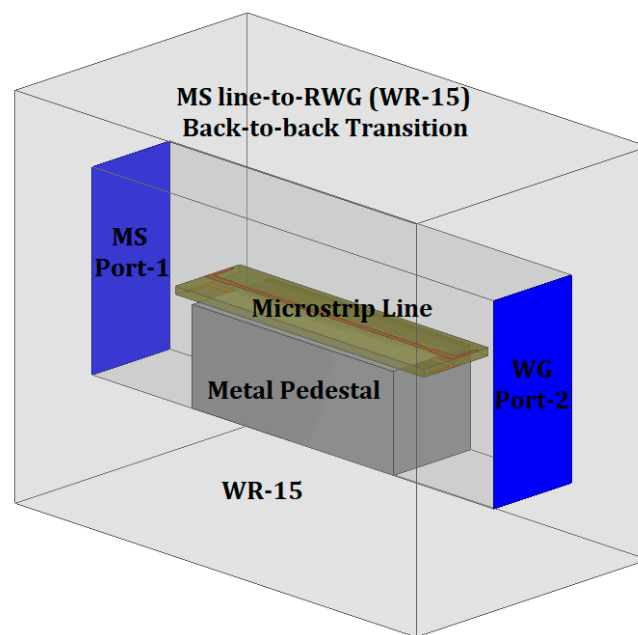
Figure 6. V-band back-to-back MS-to-WG transition.
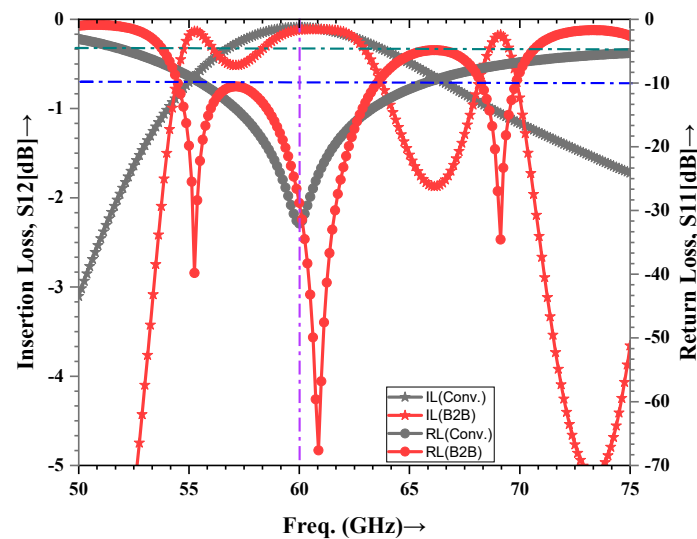
Figure 7. RL and IL plots of the conventional and B2B designed transitions.

Table 5. Resultant performance parameters of the V-band-designed MS-to-RWG transitions.

MS-to-RWG Transition	Res. Freq. f_0 (GHz)	IL (dB)	RL (dB)	FBW (%)
Conventional	60	−0.09	−32.05 (Port-1) −31.45 (Port-2)	17 (Port-1) (55.57–65.76 GHz) 10.6 (Port-2) (55.67–65.49 GHz)
Back-to-Back	55.25 60.87 69.13	−0.13 −0.12 −0.18	−39.77 −67.35 −35.36	(54.49–63.53 GHz) and (68.25–69.83 GHz)

3.1. Power Flow in the Inline MS-to-WR-15 Transition

An electromagnetic RF signal is excited through the 50 Ω microstrip line at the microstrip port and captured by the other end of the waveguide and vice versa. First, the

quasi-TEM wave starts moving from the microstrip, and then it is launched in WR-15. The impedance transformer in conjunction with the antipodal dipole antenna converts the quasi-TEM mode into the transverse electric mode (TE_{10}) of the waveguide, and, finally, power is received at the waveguide port in conventional transition, as displayed in Figure 8a.
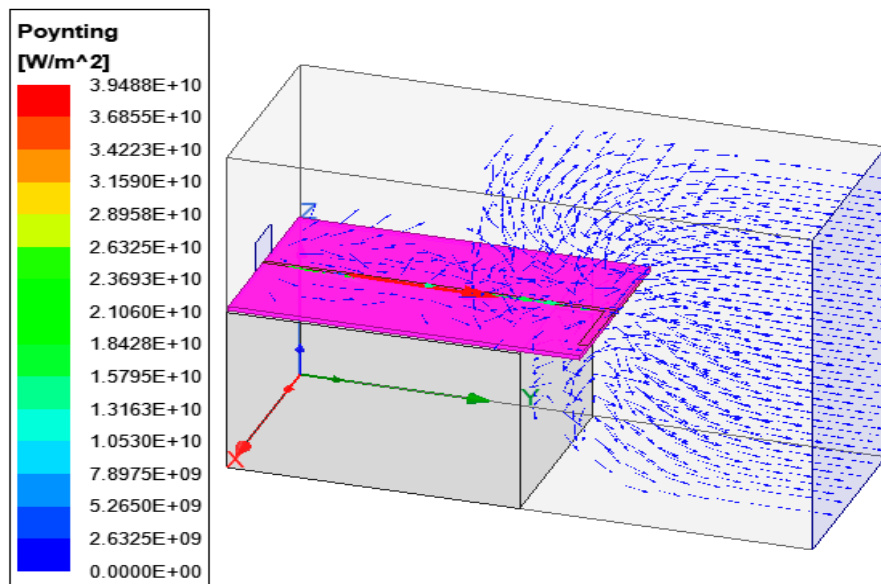
(**a**)
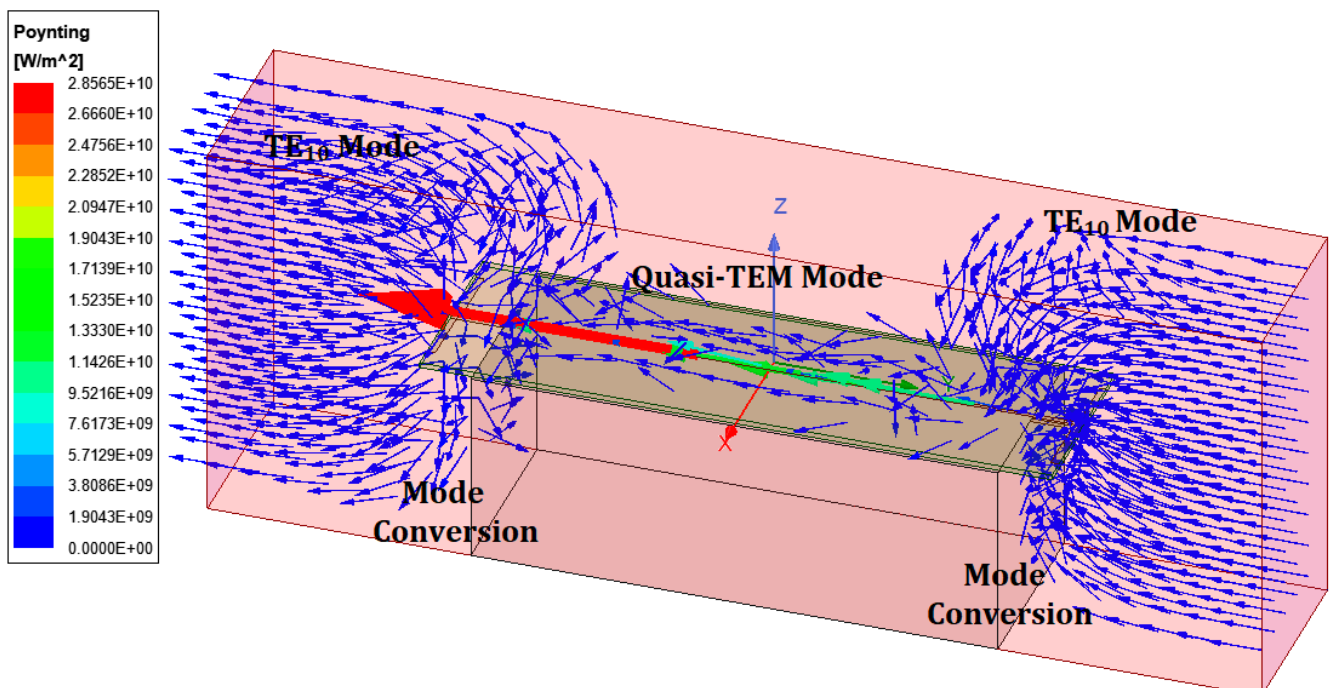
(**b**)

Figure 8. Power flow in the transition: (**a**) conventional transition and (**b**) back-to-back transition.

When two conventional transitions are connected by 180° out of phase, a back-to-back microstrip line to rectangular waveguide transition is formed. In this, the exchange of

energy is between the two waveguide ports. The RF power applied at one waveguide port by exciting the dominant TE_{10} mode is converted to the quasi-TEM mode at the microstrip interface, and then the quasi-TEM mode of the microstrip line is converted back into the TE_{10} mode at the MS line-to-RWG interface and then received at WG port-2, as represented in Figure 8b.

3.2. Electric Field Mode Conversion MS Line-to-RWG Inline V-Band Transition

Initially, when the MS line is excited by the RF signal, the quasi-TEM mode will propagate through a 50 Ω microstrip feed line, and then this mode interacts with the antipodal impedance transformer and dipole antenna arms. The impedance transformer matches the impedance of the 50 Ω microstrip feed line and antipodal dipole antenna. Finally, the electric field falls in the air medium of the rectangular WG with an impedance of approximately 500 Ω. The impedance matching between the microstrip line and RWG is compensated by the metal pedestal, impedance transformer, and InP dielectric with high permittivity (ε_r = 12.4). When the InP dielectric is entered in the RWG, the impedance of the waveguide falls to 142 Ω from 500 Ω, and the WG behaves as dielectric-filled instead of air-filled. Thus, the quarter wave transformer length and width are adjusted so that impedance matching between the MS line (50 Ω) and dielectric-filled WG (142 Ω) is achieved. When excellent matching among the two lines is achieved, the quasi-TEM mode is converted into the TE_{10} mode of the waveguide and is field-received at the WG port-2. The electric field vector distribution in the MS line-to-WG transition is depicted in Figure 9a. The VSWR plots of this inline mode converter transition are depicted in Figure 9b. The two VSWR plots from either port are found to be in concordance and have the lowest VSWR magnitude of 1.05 at a frequency of 60 GHz, for an impedance bandwidth VSWR < 2 from 55.31 GHz-to-66.11 GHz.

(**a**)
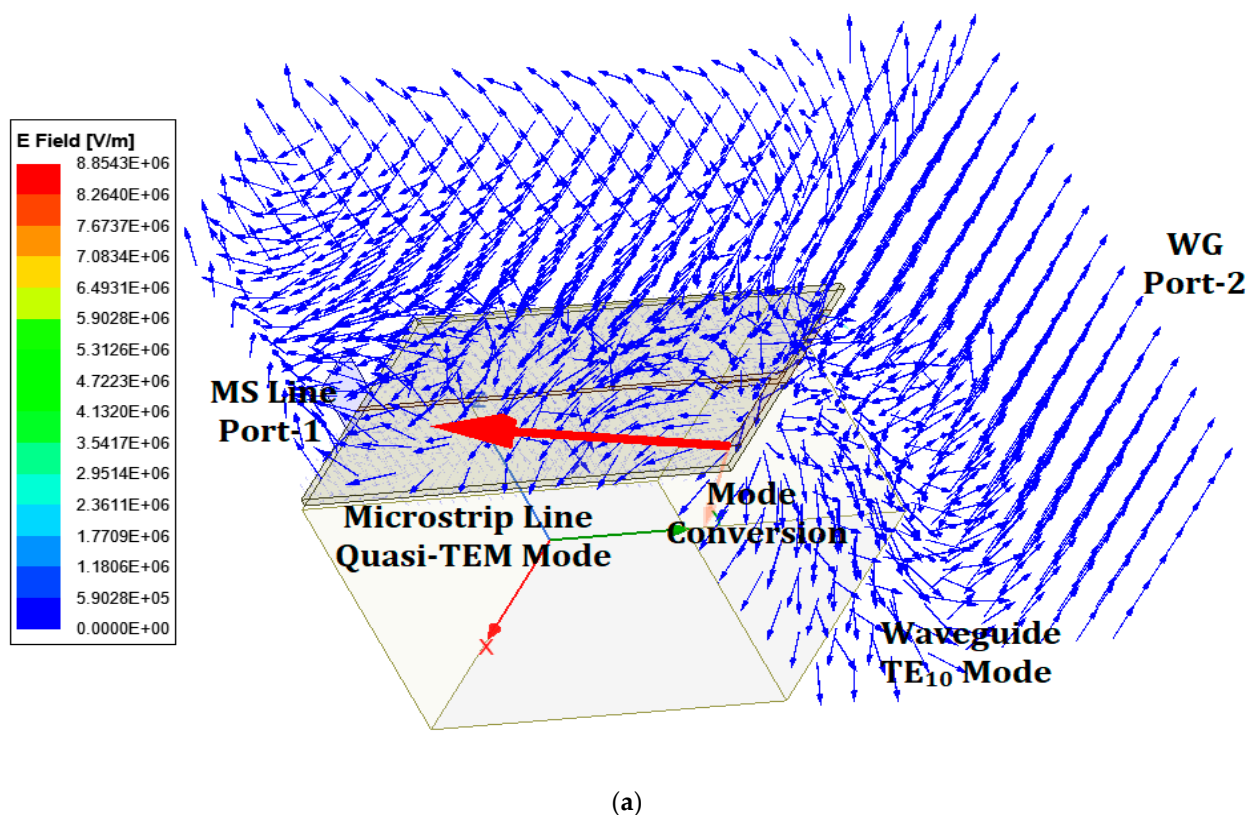
Figure 9. *Cont.*
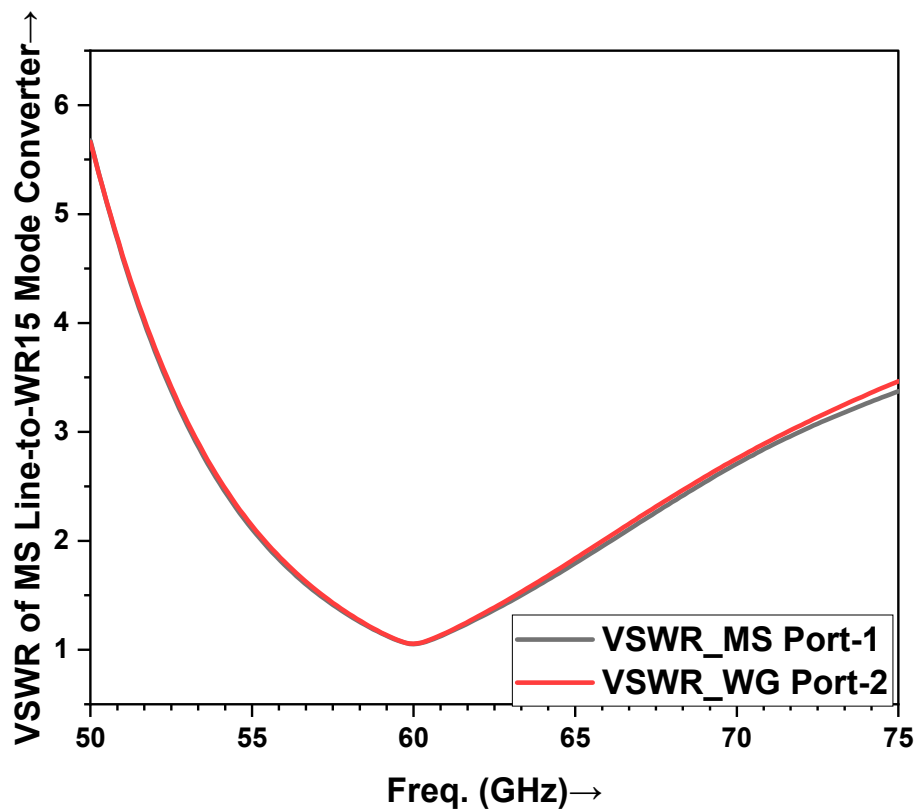
(b)

Figure 9. (**a**) Electric field mode conversion in the V-band inline MS line-to-WR-15 transition and (**b**) their VSWR plots.

3.3. Equivalent Circuit of V-Band Transition Model

The electrical equivalent circuit model of the V-band MS line-to-WR15 transition has been generated using the basic resonance theory of the RLC series and parallel circuits. Since the S_{11}/S_{22} plot of the transition has its lowest value of −31.26dB at a frequency of 60 GHz with a −10 dB fractional bandwidth of 10.18 GHz (55.53 GHz to 65.71 GHz), the transition is tuned at 60 GHz, showing that the perfectly matched inductance and capacitance values and the circuit approximately behave as a resistive circuit. The resistance of the circuit is evaluated using S_{11} (magnitude), i.e., 0.03 at 60 GHz. The quality factor of an RLC electrical resonance circuit is given by $Q = \frac{f_r}{BW}$, since the quality factor, Q, of the series resonance circuit is just the ratio of the inductive/capacitive reactance to the resistance value at resonance. Thus, the other parameter is evaluated using resonance condition $X_L = X_C$ or $L = \frac{1}{\omega^2 C}$ [32,34]. The input is connected with a microstrip line with a terminal impedance of 50 Ω, and the output is connected with the WR-15 characteristics' impedance of waveguide-dominant mode 505 Ω. The antipodal transformer and dipole antenna are replaced by parallel resistive inductive circuits. The equivalent circuit is plotted using the ADS RF circuit simulator, as shown in Figure 10a. The S_{11} result of the circuit simulator shows excellent agreement in terms of fractional bandwidth, return loss, and tuning frequency with the simulated results, as displayed in Figure 10b,c.
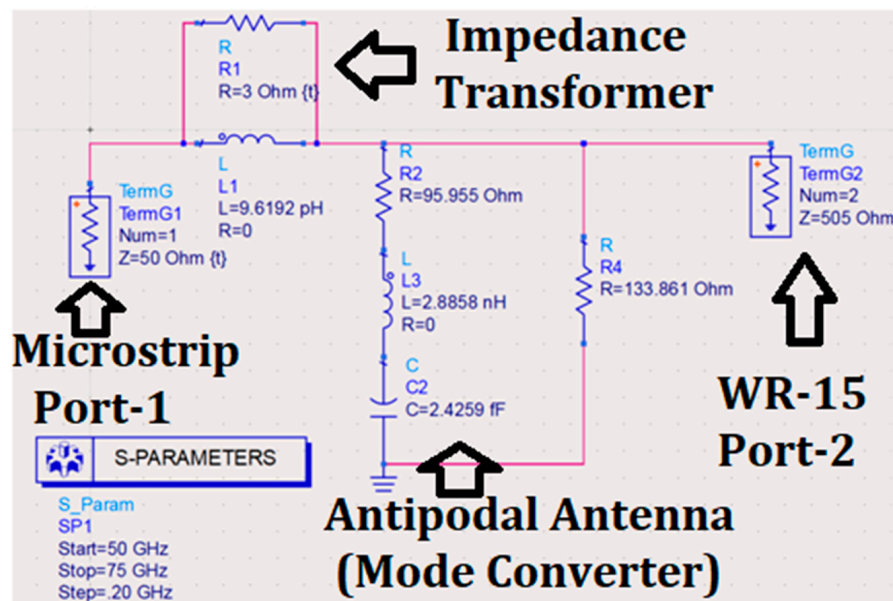
(**a**)
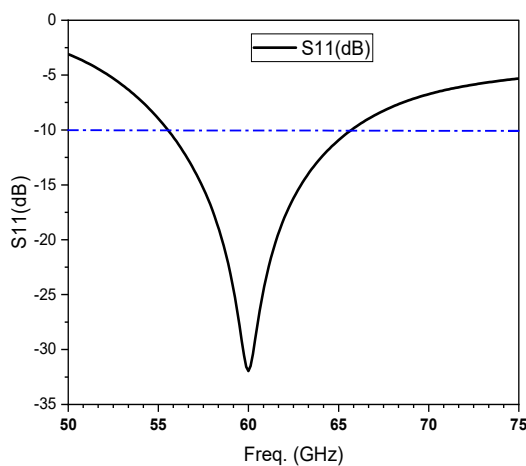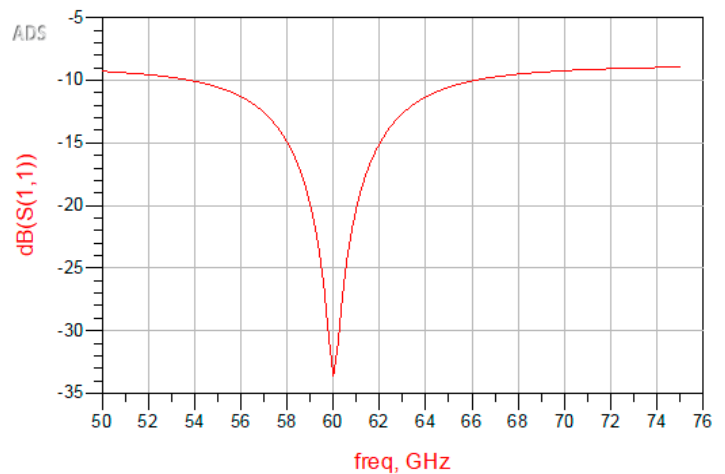
(**b**)   (**c**)

Figure 10. Electrical equivalent circuit of the proposed MS line-to-waveguide transition model: (**a**) electrical equivalent circuit of the model, (**b**) HFSS reflection coefficient plot, and (**c**) validation of electrical equivalent circuit model using ADS RF circuit simulator.

3.4. Performance Comparison of V-Band Transitions

The comparisons of the proposed design with the previously published work of the V-band have been listed in Table 6 in terms of the MS-to-RWG performance parameters. The proposed design is simple, compact, and easier to fabricate on double-etched layered PCB for microstrip lines. The RL, IL, and −10 dB FBW of the proposed design are better than the existing designs, and [18,23,27,29] show the −10 dB fractional bandwidths. The proposed design is well-resonated at the V-band center frequency of 60 GHz.

Table 6. Performance comparison of proposed V-band (50 GHz–75 GHz) transitions with the existing literature.

Ref.	Substrate Used for MSL	RWG Type ('a' mm × 'b' mm) and WallThickness (t mm)	RL < (dB)	IL > (dB)	FBW (%)	Coupling Method and Features
[18] Shih, Y. C. et al. 1988	RT-Duriod 5880 ε_r = 2.2 h = 0.127 mm $\tan\delta \approx 0.0009$ at 10 GHz	WR-12 (3.10 × 1.55) t = 1.015	−12	−1.0	40 (relative BW)	.Transverse (90°) .Microstip probe as launcher .Aperture cut
[23] Aliakbarian et al. 2010	Rogers RT/Duroid 5880 ε_r = 2.2 h = 0.254 mm $\tan\delta$ = 0.0009 10 GHz	WR-15 (3.76 × 1.88) t = 1.015	−17	−4.0	37.7	.End-wall .Consists of an end-wall .A double-sided etched substrate .Slot coupling
[25] Zhou, I., and Robert, J. R. 2022	RO4003 ε_r = 3.55 h = 0.81 mm $\tan\delta$ = 0.002	WR-34 (4.5 × 8.8) t = 2.0	−17, −30	−0.67, −0.85	21.2, 23	.Inline .LMDS, Ka-band operation for 5G applications
[26] Kyu, Y.H. and Pao, C. 2012	Quartz ε_r = 3.8 h = 0.127 mm $\tan\delta$ = 0.0009	WR-15 (3.76 × 1.88) t = 1.015	−37	−0.7 (B2B) −0.35 (conv.)	35.2	.Inline (E-plane) .Five-step ridge waveguide .Probe fed .Broad band
[27] Mozharovskiy A. V., 2019	RO4350B ε_r = 3.66 H = 0.101 mm $\tan\delta$ = 0.0115 at 60 GHz RT/Duroid 5880 ε_r = 2.2 H = 0.127 mm $\tan\delta$ = 0.0024 at 60 GHz	WR-15 (3.76 × 1.88) t = 1.015	−10 −10	−1.1 −0.4	11.2 20	.Transverse B2B .Low loss .Wideband .Uses 25 via
[28] Xu, Z. et al. 2021	Quartz ε_r = 3.78 h = 0.127mm $\tan\delta$ = 0.0024	WR-10 (2.54 × 1.27) t = 1.015	−18	−0.35 to −0.5	31.89	.W-band inline B2B E-plane probe T-junction structure .mm-wave applications
[29] Henderson, J. R. and Walden, M. C. 2022	RT/Duroid 5880 ε_r = 2.2 h = 0.127mm $\tan\delta$ = 0.0024	WR-15 (3.76 × 1.88) t = 1.015	−10	−1.0	21.87	.Inline .PCB transition .Highly integrated with mm-wave beam-forming devices .3D-printed mm-wave sectoral horn array
This work	InP ε_r = 12.4 h = 50 μm $\tan\delta$ = 0.0001 at 60GHz	WR-15 (3.76 × 1.88) t = 1.015	−30	−0.09	40.76 (relative BW)	.Inline (0°) .Dipole antipodal antenna as launcher .Double-sided etched InP substrate

4. Discussion

Two microstrips to rectangular waveguide transitions are proposed: one conventional inline transition and another back-to-back transition. Both designs possess reflection coefficient (RL) values lower than −10 dB with maximum transmission coefficients (S_{21}). The S_{21} value in back-to-back transitions is approximately double within the relative bandwidth of 40.76%. This ensures that the additional dielectric losses, waveguide-wall copper losses, and radiation losses may improve, and this may stop the wave from propagating along the two waveguide ports. Both transitions have IL better than −0.50 dB; thus, most transmission takes place with minimum reflections in the V-band. Therefore, the proposed inline V-band transition is suitable for MIC/MMIC circuit characterization.

5. Conclusions

An inline microstrip to rectangular waveguide transition has been presented in this paper for V-band applications. The electrical equivalent circuit of the model has been generated, and its reflection coefficients are found to be in agreement with simulated reflection coefficients. The design is simple and compact in structure, as no complicated ridge, stepped waveguide, or waveguide back-short were used in the design. This makes the design economic and easy to fabricate using micromachining methods. An antipodal dipole microstrip antenna is used for far-field energy coupling in the RWG. A high permittivity InP substrate of 50 μm thickness is used for the microstrip instead of the costly 127 μm or 254 μm thick Roger/RT Duroid 5880; this reduces the radiation and dielectric losses,

and a metal pedestal is used to support the microstrip line inside the waveguide WR-15 and plays the role of the ground for the microstrip antenna. No external unit is needed for the proposed inline transition. Therefore, the transition length is equal to the WR-15 length. It can be noticed that by reducing the thickness, the substrate reduces the fractional bandwidth by small extents of the transition, improves the transmission, and reduces the reflections within the transition ports. The designed transition is most suitable for mm-wave communication, interconnects for front end in receivers/transmitters, MMIC/MIC circuits, unlicensed devices (59–64 GHz), the ISM band (61.25 GHz $\pm$ 0.25 GHz), Earth exploration satellites, Inter-SAT, fixed satellite locations, space research, and missile navigation applications. This method could be generalized to create any band of inline MS-to-WG Transitions.

Author Contributions: Conceptualization, A.V. and V.S.; methodology, A.V. and I.E.; software, A.V., C.Z. and Z.V.; validation, A.V. and V.S.; formal analysis, A.V. and I.E.; investigation, A.V. and C.Z.; resources, A.V.; writing—original draft preparation, A.V.; writing—review and editing, A.V., J.R. and V.S.; visualization, V.S.; supervision, V.S.; funding, J.R. and Z.V. All authors have read and agreed to the published version of the manuscript.

Funding: This project received funding from the European Union's Horizon 2020 research and innovation program under grant agreement H2020-MSCA-RISE-2018-EXPLOR-872897. This work is also funded by the FCT/MEC through national funds and when applicable co-financed by the ERDF, under the PT2020 Partnership Agreement under the UID/EEA/50008/2020 project.

Data Availability Statement: The authors declare that all data are provided in the article.

Acknowledgments: The authors would like to express their sincere thanks to the Honorable Vice-Chancellor, GK (DU), Haridwar, Uttarakhand, India, for his motivation and encouragement regarding the research and for providing the simulation and laboratory environment for conducting the research work.

Conflicts of Interest: The authors declare no conflict of interest.

References

1. Hassan, S.E.; Berggren, M.; Scheiner, B.; Michler, F.; Weigel, R.; Lurz, F. Design of planar microstrip-to-waveguide transitions using topology optimization. In Proceedings of the 2019 IEEE Radio and Wireless Symposium (RWS), Orlando, FL, USA, 20–23 January 2019; pp. 1–3.
2. Ren, Y.; Li, K.; Wang, F.; Gao, B.; Wu, H. A broadband magnetic coupling microstrip to waveguide transition using complementary split ring resonators. *IEEE Access* **2019**, *7*, 17347–17353. [CrossRef]
3. Huang, X.; Wu, K.-L. A broadband U-slot coupled microstrip-to-waveguide transition. *IEEE Trans. Microw. Theory Technol.* **2012**, *60*, 1210–1217. [CrossRef]
4. Deslandes, D.; Wu, K. Integrated microstrip and rectangular waveguide in planar form. *IEEE Microw. Wirel. Compon. Lett.* **2001**, *11*, 68–70. [CrossRef]
5. Pérez-Escudero, J.M.; Torres-García, A.E.; Gonzalo, R.; Ederra, I. A Gap Waveguide-based compact rectangular waveguide to a packaged microstrip inline transition. *Appl. Sci.* **2020**, *10*, 4979. [CrossRef]
6. Pérez, J.M.; Rebollo, A.; Gonzalo, R.; Ederra, I. An inline microstrip-to-waveguide transition operating in the full W-Band based on a Chebyshev multisection transformer. In Proceedings of the European Conference on Antennas and Propagation (EuCAP), Davos, Switzerland, 10–15 April 2016; Volume 10, pp. 1–4.
7. Pérez-Escudero, J.M.; Torres-García, A.E.; Gonzalo, R.; Ederra, I. A simplified design inline microstrip-to-waveguide transition. *Electronics* **2018**, *7*, 215. [CrossRef]
8. Simone, M.; Fanti, A.; Valente, G.; Montisci, G.; Ghiani, R.; Mazzarella, G. A compact in-line waveguide-to-microstrip transition in the Q-Band for radio astronomy applications. *Electronics* **2018**, *7*, 24. [CrossRef]
9. Li, C.L.; Jin, C.; Ma, H.Q.; Shi, X.W. An inline waveguide-to-microstrip transition for wideband millimeter-wave applications. *Microw Opt. Tech Lett.* **2015**, *62*, 1516–1520. [CrossRef]
10. Hügler, P.; Chaloun, T.; Waldschmidt, C. A wideband differential Microstrip-to-Waveguide Transition for multilayer PCBs at 120 GHz. *IEEE Microw Wirel. Compts Lett.* **2020**, *30*, 170–172. [CrossRef]
11. Kaneda, N.; Qian, Y.; Itoh, T. A broad-band Microstrip-to-Waveguide Transition using quasi-Yagi Antenna. *IEEE Trans. Microw. Theory Techn.* **1999**, *47*, 2562–2567. [CrossRef]
12. Van Heuven, J.H.C. A new integrated Waveguide-Microstrip Transition. *IEEE Trans Microw Th. Tech.* **1976**, *24*, 144–147. [CrossRef]
13. Lou, Y.; Chan, C.H.; Xue, Q. An in-line Waveguide-to-Microstrip Transition using radial-shaped probe. *IEEE Microw Wirel. Compts Lett.* **2008**, *18*, 311–313. [CrossRef]

14. Tang, C.; Pan, X.; Cheng, F.; Lin, X. A broadband Microstrip-to-Waveguide end-wall probe transition and its application in waveguide termination. *Progr. Electromagnet Res. Lett.* **2020**, *89*, 99–104. [CrossRef]

15. Varshney, A.K. A microwave rectangular waveguide-to-microstrip line transitions @30 GHz. *Inter. J. Emerg. Tech. Ad. Eng.* **2013**, *3*, 1–6.

16. Gupta, R.; Kumar, P.P. Improved design of Ka-band waveguide to coaxial right angle microwave transition. In Proceedings of the 2020 URSI Regional Conference on Radio Science (URSI-RCRS), Varanasi, India, 12–14 February 2020.

17. Ariffin, A.; Isa, D. Bandwidth enhancement of microstrip line-to-waveguide transitions for broadband E-band module applications. *Microw. Opt. Tech. Lett.* **2016**, *58*, 1398–1401. [CrossRef]

18. Shih, Y.C.; Ton, T.N.; Bui, L.Q. Waveguide-to-Microstrip Transitions for mm-wave applications. In Proceedings of the IEEE MTT-S International Microwave Symposium Digest, New York, NY, USA, 25–27 May 1988; pp. 473–475.

19. Murphy, E.R. Microstrip to Waveguide Transition. U.S. Patent 4453142, 5 June 1984.

20. Lin, T.-H.; Wu, R.-B. A Broadband Microstrip-to-Waveguide transition with tapered CPS probe. In Proceedings of the 32nd European Microwave Conference, Milan, Italy, 23–26 September 2002; pp. 1–4.

21. Varshney, A.; Sharma, V. A comparative study of microwave rectangular waveguide-to-microstrip line transition for millimeter wave, wireless communications and radar applications. *Microw. Rev.* **2020**, *2*, 26–37.

22. Sakakibara, K.; Hirono, M.; Kikuma, N.; Hirayama, H. Broadband and planar microstrip-to-waveguide transitions in mm-wave band. In Proceedings of the 2008 International Conference on Microwave and Millimeter Wave Technology, Nanjing, China, 21–24 April 2008; pp. 1278–1281.

23. Aliakbarian, H.; Enayati, A.; Vandenbosch, G.A.E.; De Raedt, W. Novel Low-Cost End-Wall Microstrip-To-Waveguide Splitter Transition. *Prog. Electromagn. Res.* **2010**, *101*, 75–96. [CrossRef]

24. Kumari, S.; Mondal, P. Full U-Band Rectangular Waveguide-to-Microstrip Transition Using E-Plane Probe. In Proceedings of the 11th International Radar Symposium India—2017, Bangalore, India, 12–16 December 2017; pp. 1–4.

25. Balani, C.A. *Antenna Theory*, 4th ed.; Wiley: New York, NY, USA, 2016.

26. Pozar, D.M. *Microwave Engineering*, 4th ed.; Wiley: New York, NY, USA, 2016; pp. 148–149.

27. Varshney, A.; Cholake, N.; Sharma, V. Low-cost ELC-UWB fan-shaped antenna using parasitic SRR triplet for ISM band and PCS applications. *Int. J. Electron. Lett.* **2021**, *10*, 391–402. [CrossRef]

28. Liao, S.Y. *Microwave Devices and Circuits*, 3rd ed.; Pearson Prentice Hall: Hoboken, NJ, USA, 2007.

29. Theraja, B.L. *A Textbook of Electrical Technology (Basic Electrical Engineering)*; S. Chand Publishing: New Delhi, India, 2005; Volume 1.

30. Zhou, I.; Robert, J.R. Ultra-Wideband Narrow Wall Waveguide-to-Microstrip Transition Using Overlapped Patches. *Sensors* **2022**, *22*, 2964. [CrossRef] [PubMed]

31. Han, K.Y.; Pao, C. A V-band waveguide to microstrip inline transition. In Proceedings of the IEEE/MTT-S International Microwave Symposium Digest, Montreal, QC, Canada, 17–22 June 2012; pp. 1–3.

32. Mozharovskiy, A.V.; Soykin, O.V.; Artemenko, A.A.; Maslennikov, R.O.; Vendik, I.B. Wideband Wave-guide-to-Microstrip Transition for mm-Wave Applications. *J. Russ. Universities. Radioelectron.* **2019**, *22*, 17–32. [CrossRef]

33. Xu, Z.; Xu, J.; Qian, C. Novel In-Line Microstrip-to-Waveguide Transition Based on E-Plane Probe T-Junction Structure. *IEEE Microw. Wirel. Compon. Lett.* **2021**, *31*, 1051–1054. [CrossRef]

34. Henderson, J.R.; Walden, M.C. Microstrip-to-Waveguide Transition for 3D-Printed mm-Wave Sectoral Horn Array. In Proceedings of the 16th European Conference on Antennas and Propagation (EuCAP), Madrid, Spain, 27 March–1 April 2022; pp. 1–3.